Hindawi
International Transactions on Electrical Energy Systems
Volume 2023, Article ID 8830451, 14 pages
https://doi.org/10.1155/2023/8830451

Research Article

Improved Dynamic Response of a Single-Phase-Integrated KY Boost Converter with an MLI System of a DC-AC Converter in Motor Speed Regulation

V. Mohan and K. Nandakumar

Department of Electrical and Electronics Engineering, E.G.S. Pillay Engineering College, Nagapattinam, Tamilnadu 611002, India

Correspondence should be addressed to K. Nandakumar; nandakumar071974@gmail.com

Received 11 April 2023; Revised 19 October 2023; Accepted 13 November 2023; Published 28 November 2023

Academic Editor: Paulo Moisés Almeida Costa

KY boost converter (KBC) finds wide application in photovoltaic (PV) and single-phase inverters. In this study, a novel KBC containing seven levels of a multilevel inverter (MLI) is presented. Here, KBC between the direct current (DC) source and the inverter is proposed. Moreover, the authors considered a closed-loop response of the KBC-MLI system with a proportional integral (PI) controller and a fractional-order PID (FOPID) Controller. The main purpose of this suggested technique is to match the output current, total harmonic distortion (THD), and dynamic response of closed-loop PI and FOPID-controlled KBC-MLI systems. The proposed model is simulated with the MATLAB software, and the attained outcome illustrated an enhanced dynamic performance by using the FOPID-controlled KBC-MLI system. The simulation results of the KBC-MLI technique have been evaluated against the theoretical models. Finally, extensive experiments were carried out to validate the theoretical results.

1. Introduction

KBC is a DC-DC boost converter that has been evidently modified form of a canonical switching converter (CSC) [1] or topology alterations being carried out over DC-DC-BC [2]. The modifications in CSC possessing yield inductors have resulted in KBC [3–7]. The yield and input flows possess substantial current ripples that are deemed to be an impediment to the CSC-converter. In the increase of inductance at the conversion stage, the resultant structure is a genuine switched mode (SM) topology. In order to lower inductance, the resonant switching mode was applied to this topology. These results in low-yield ripple current in the DC-connect. Considering the existing DC-DC converters, the inductor capacitor (LC) satisfies the ideal inverter which has the lowest number of components but has elevated input and yield current ripple execution of the framework compared to other converters like an ordinary buck-boost Converter (BBC). The proposed LC topology has a noteworthy feature in which the current ripples at the inputs and yields are decreased.

Induction motors (IMs) are most utilized in the industry since they are rough, reasonable, and without support. It is evaluated that over half of the world's electric energy created is devoured by electric machines. Enhancing proficiency in electric drives is critical, predominantly for monetary sparing and decrease of natural contamination [8, 9]. IM has high effectiveness at evaluated speed and torque. In any case, at light loads, engine proficiency diminishes significantly because of the occurrences of irregularities among copper. Consequently, power reduction could be accomplished using an appropriate choice of engine transition levels [10, 11].

IM has been employed for carrying out several tasks, for example, warming, aeration, and refrigeration, electrical drives such as motion control, robotics, and automotive controls such as electric vehicles [12] [13]. The induction motor drive (IMD) can be controlled by various execution capacities, for example, input control, speed, torque, air-gap motion, power factor, stator flow, and stator voltage in general productivity [2].

For electrical household appliances such as mechanical siphons, motorized fans, and wind blowers, single-stage machines frequently get coupled to single-phase power systems [14]. Whenever the electrical source's frequency is constant, induction motors (IMs) may be used for a stable performance. It is a variable speed in application machines with the progression of intensity gadgets by creating a three-phase-supply of adjustable recurrence as well as potential energy with pulse width modulation (PWM) [15] procedures connected to a solid-state inverter (SSI) [16].

Three-stage IM is generally utilized in boost and vehicle applications for a considerable length of time on account of its moderately basic structure, which supports free activity and capacity to begin specifically from the supply start-up. The deployment machine's superior elements are accomplished by the field orientation control (FOC). The three-stage induction motor FOC (IMFOC) utilizes the perplexing exchange work idea to tune the PI controller by utilizing the recurrence reaction capacity of the closed-loop complex exchange capacity of the controlled IM.

2. Research Gap

The abovementioned research works do not concentrate more on the use of motors in AC loads. This research work proposes the motor for AC loads. The KBC-MLI system, AC loads utilizing PI control devices, or FOPID control systems have been excluded in the aforementioned research. In the present investigation, PI as well as FOPID controllers for the KBC-MLI system that manages AC loads is compared. Increased power output and less ripple voltages, along greater reaction times, are all possible using the KY boost converters. The KY boost converter is modeled and simulated in constant output, and better speed regulation is included in this paper. In this article, a modified phase shifted-level pulse width modulation (PWM) for a 7-level inverter is utilized.

3. System Description

3.1. PI Controller. This constitutes a composite controlling mechanism that is created by combining integral and proportional modes. The key advantage of this mode of operation is the fact that it achieves a direct link between the proportional and integral modes, eliminating the difference between them and allowing the outcome to be reverted to zero inaccuracies in the event of load fluctuation.

3.2. FOPID Controller. Fractional differentiation has been employed to create the FOPID model. In comparison to a similar PI control structure, the reaction utilizing FOPID is quicker. Figure 1 shows a block diagram that represents the FOPID control mechanism. A FOPID controller's transfer function has a structure of

$$C_{F.O.P.I.D}(s) = K_p + \frac{K_i}{s^{\lambda}} + K_d s^{\mu}, \tag{1}$$

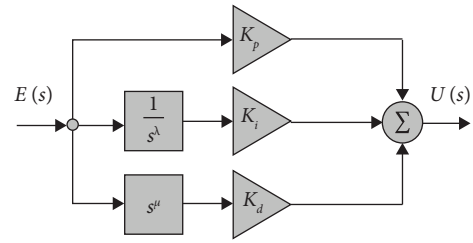

Figure 1: Block diagram of the FOPID controller.

where λ corresponds to the integral part order and μ represents the derivative part order, whereas K_p, K_i, and K_d signify the controller similar to the traditional PID controller.

The DC output has been measured and assessed against standard output voltage providing the error signal which is discharged by the PID for withstanding the motor speed outcome as constant as well as reducing the steady-state error. The set current is compared with the actual current. The FOPID parameters, proportional gain (Kp), and double integral times (Ti) have been evaluated utilizing the Zeigler–Nichols tuning process. The schematic articulation of the closed-loop KBC-MLI system with a PI controller is shown in Figure 2.

The elementary expression for the KY boost voltage ratio is represented as

$$V_o = V_i \frac{T_{\text{on}}}{T_t}, \tag{2}$$

where V_o = output voltage in volt, V_i = input voltage in volt, T_{on} = on time in seconds, and T_t = total time in seconds.

The representation of FOPID is derived from the fractional differential equations. The output of FOPID is quicker when compared with the equivalent PI control technique. FOPID control system transfer function shall be expressed as

$$C_{\text{FOPID}} = K_p + \frac{K_i}{S^{\lambda}} + K_d S^{\lambda}, \tag{3}$$

where λ corresponds to the integral part order and μ represents the derivative part order, whereas K_p, K_i, and K_d signify the controller similar to the traditional PID controller.

The DC yield voltages are sensed and assessed against reference yield voltage that offers error signals. Output motor speed is controlled by this error signal, and steady-state error gets reduced. The set speed is compared with the actual speed. The FOPID parameters, proportional gain (K_p), and double integral times (T_{is}) have been calculated utilizing the Zeigler–Nichols tuning technique. The schematic representation signifying the FOPID control system has been shown in Figure 3.

The DC yield voltage has been sensed and assessed against the standard yield motor speed providing the error signals. These error signals are processed using the FOPID for sustaining the resultant motor speed constants as well as diminishing the steady-state errors. The schematic representation of the closed-loop KBC-MLI system of a DC-AC converter with a motor is shown in Figure 4.

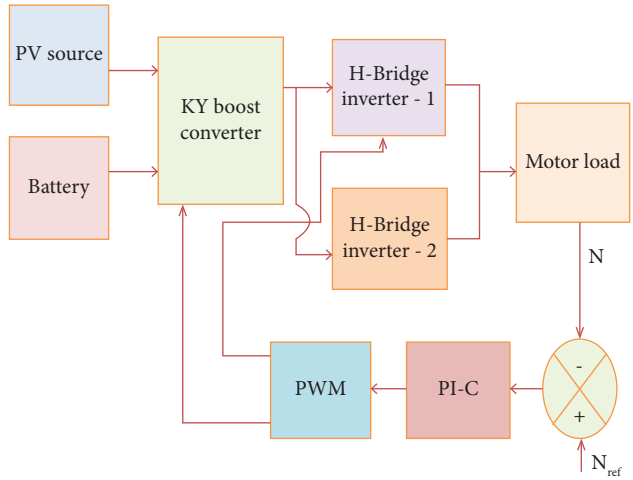

Figure 2: KBC-MLI system with a PI controller.

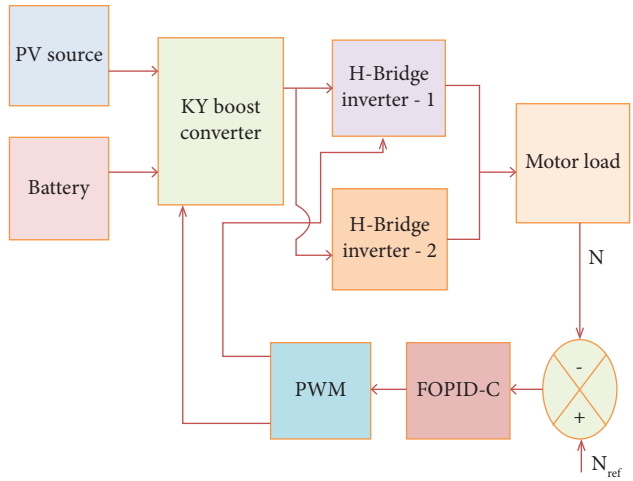

Figure 3: KBC-MLI system with a FOPID controller.

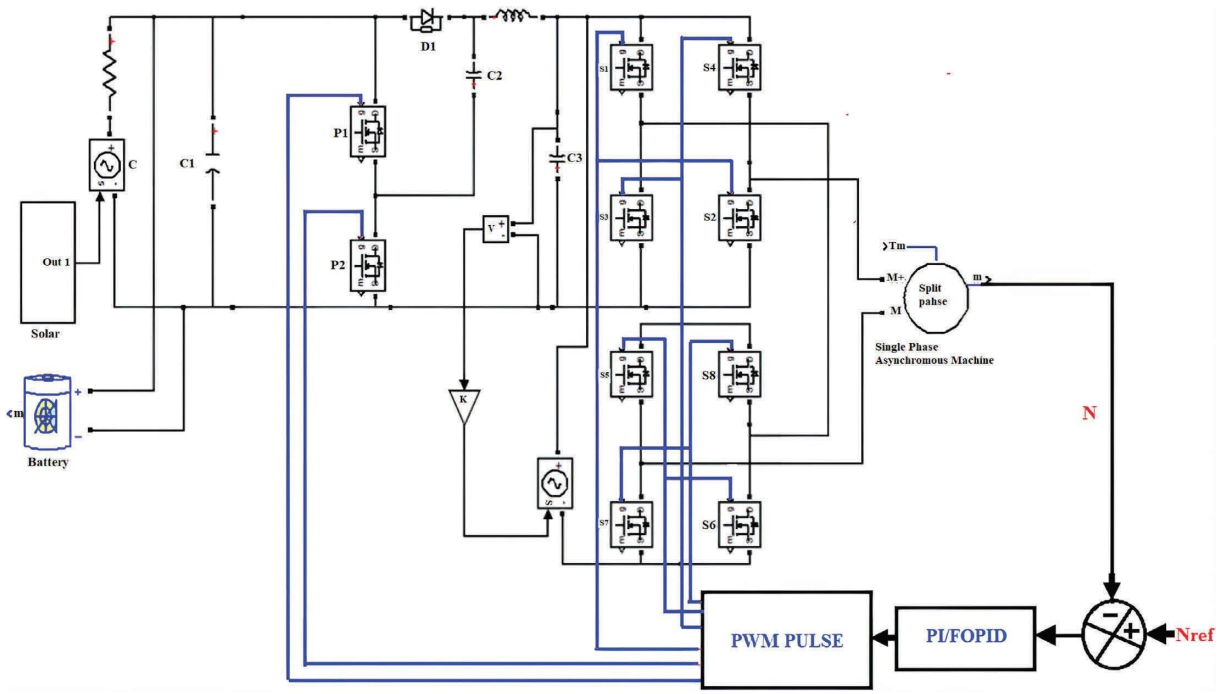

Figure 4: Closed-loop KBC-MLI structure with a PI and FOPID controller.

While achieving a reduced current THD [17–20], voltage with increased motor speed regulations for satisfying the appropriate standards is attained. The speed, as well as current regulators, was utilized for regulating the output current sequence for PI and FOPID-controlled validation of KBC as well as MLI systems. This research work focuses on the reduced output current THD and speed regulation of the KBC-CMLI system concerning an AC-DC converter with a motor load network.

In this study, two H-bridge systems were used. 1 : 2 voltage ratios are used to get the seven-level output in this system. The resulting voltage from the CHB inverter regulated employing MSF PWM via the equivalent dc-link voltage ratio (1/2 Vdc: 1/2 Vdc) has the fewest low-order harmonics, whereas the resultant voltage from the CHB inverter regulated utilizing PWM with a disproportionate dc-link voltage ratio (2/3 Vdc: 1/3 Vdc) possesses seven levels. The quantity of accessible values for the resultant voltage continues to increase, which is in accordance with the overall level of the voltage that is produced. In this case, a 2-cell H-bridge inverter with 8 switches is all that is required to provide a voltage output with 7 levels.

The main contribution of this paper is to reduce output current THD and motor speed dynamic response of closed-loop PI and FOPID-controlled KBC-MLI systems. The better response of the FOPID controlled system can be seen in Tables 1 and 2.

4. Results and Discussion

4.1. Open-Loop KBC-MLI. The open-loop source disturbances of the KBC-MLI structure have been represented in Figure 5. The input voltage of the open-loop KBC-MLI structure has been displayed in Figure 6, and the voltage across PV is increased from 48V to 54V. The output voltage of KBC-MLI is shown in Figure 7, and the output voltage is 165V. The output voltage across the motor load of the KBC-MLI structure has been displayed in Figure 8, and the inverter output voltage is 165V. The output current of the KBC-MLI system is depicted in Figure 9, and the output current of the KBC-MLI system is 10A. In lower load resistance, a high load current is achieved. The output current THD of the motor load is described in Figure 10 with the value being 12.27%. For higher order harmonics, THD gets reduced. The motor speed of the KBC-MLI system is displayed in Figure 11, and the value of motor speed in the KBC-MLI system is 1150 rpm from completing 1 second onwards. The motor torque of the KBC-MLI structure has been shown in Figure 12, and the value of motor torque in the KBC-MLI system is 5.3 N-m. Motor torque starts to settle from 1.1 seconds onwards. The motor's generated torque rises quickly towards the highest possible level before leveling out at its level of stability.

4.2. KBC-MLI System with a Closed-Loop PI Controller. Figure 13 displays the schematic representation of closed-loop KBC-CMLI utilizing a PI controller. Input voltage across the PV has been represented in Figure 14; the voltage across the PV is increased from 48V to 54V. The output voltage of the KBC-MLI structure is represented in Figure 15; the output voltage value is 150V. The motor load voltage is displayed in Figure 16; the motor load voltage is 150V. The motor load current has been articulated in Figure 17; the value of current through the motor load is 16A. The output current THD of the motor load is described in Figure 18 with 8.42%. Motor speed and zoom-out are delineated in Figures 19 and 20, respectively; the motor speed is 1050 rpm. Motor torque is shown in Figure 21; 5.1 N-m is the motor torque value.

Table 1: Comparative analysis of time-domain parameters (motor speed) of KBC-MLI with a PI controller and FOPID controller.

Type of controller	$T_{r(\text{sec})}$	$T_{p(\text{sec})}$	$T_{s(\text{sec})}$	$E_{\text{ss}(\text{sec})}$
PI	1.12	1.15	3.80	6.3
FOPID	1.09	1.10	3.10	5.2

Table 2: Assessment of output current THD.

KBC-MLI	Output current THD (%)
Without a controller	12.27
With a PI controller	8.42
With a FOPID controller	5.21

The PWM approach has been employed in the present investigation to regulate the acceleration of a single-phase induction motor utilizing FOPID. Using an optimized inductive motor type, the PWM-generated output serves as the basis for a voltage source inverter having a desirable duty cycle. The development of a method of control for producing controlled PWM signals. The motor speed response created the system's steady-state error as well as settling time found to be within the prescribed speed control limits, according to the findings. The motor speed responses of PI and FOPID-controlled system results are included in Figures19 and 22.

4.3. KBC-MLI System with a Closed-Loop FOPID Controller. Closed-loop KBC-MLI using the FOPID controller has been illustrated in Figure 23. Figure 24 illustrates the input voltage across the solar PV, and the value of solar PV voltage is increased from 48 V to 54 V.

The voltage across the motor load is delineated in Figure 25; the value is 150 V. Figure 26 shows the current through the motor load, and the value is 16A. Output current THD of the motor load is described in Figure 27 with 5.21%. Motor speed and zoom-out are depicted in Figures 28 and 22, respectively; the motor speed is 1050 rpm. Motor torque is shown in Figure 29 with 5.1 N-m.

Table 1 compares the time domain with PI and FOPID controller parameters. By using FOPID, the rise time has been seen to be lowered from 1.12 to 1.09 secs; the settling time has been seen to be lowered from 1.15 to 1.10 secs; similarly, the peak time has been seen to be lowered from 3.80 to 3.10 secs; the steady-state error has been lowered from 6.3 to 5.2 rpm. The graphical illustration of time-domain responses is presented in Figure 30. Table 2 represents the assessment of the output current THD without a controller, with PI, and FOPID

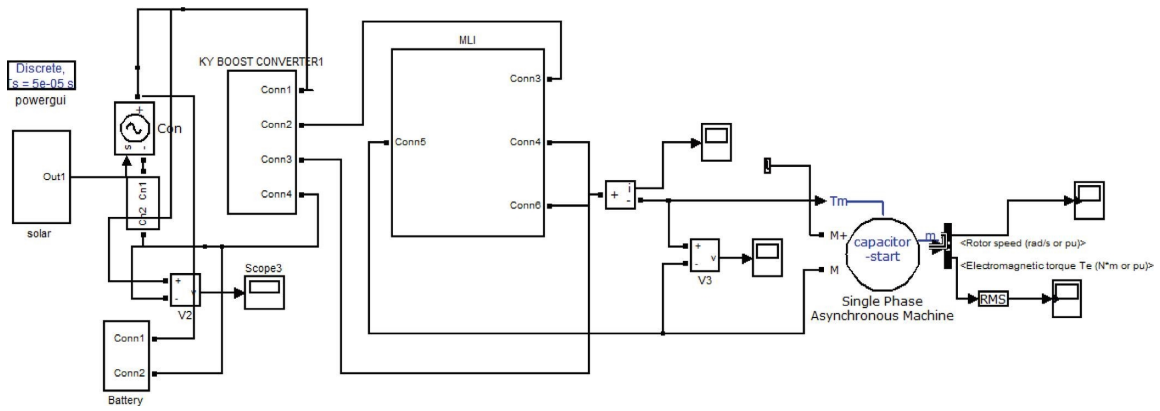

Figure 5: Circuit diagram of the closed-loop KBC-MLI system with source disturbance.

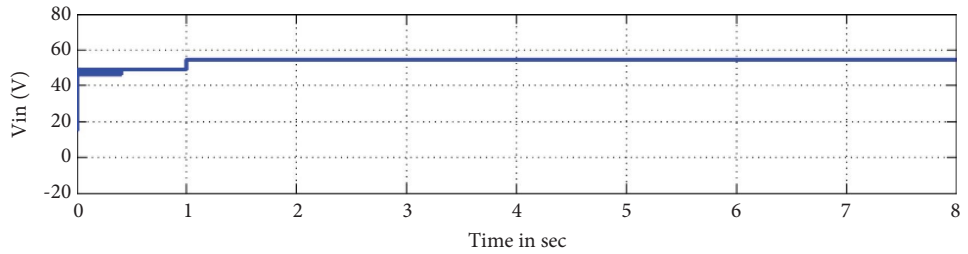

Figure 6: Solar PV voltage.

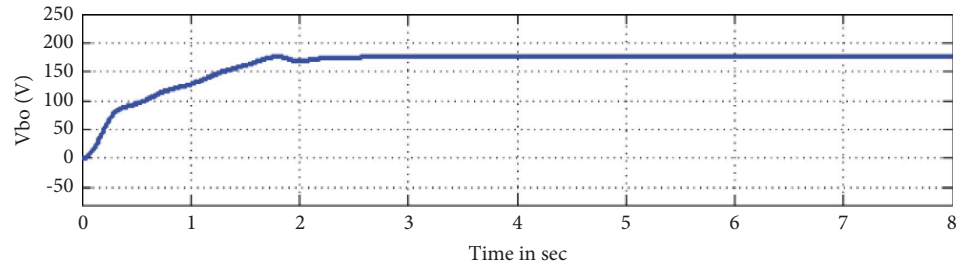

Figure 7: Output voltage across the motor of the closed-loop KBC-MLI system with source disturbance.

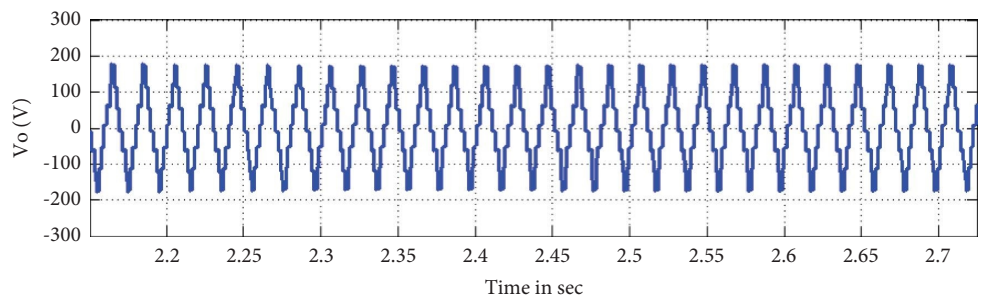

Figure 8: Output voltage across the motor of the closed-loop KBC-MLI system source disturbance.

controller, and the bar chart for THD response is shown in Figure 31. Hence, closed-loop KBC-MLI with a FOPID controller is superior to closed-loop KBC-MLI with a PI controller system.

In the present study, a multilayer inverter has been developed utilizing 8 switches as well as dual 1 : 2 dc-link voltages. The suggested architecture is also capable of producing voltages across seven stages with the right gate inputs. In cascaded 7-

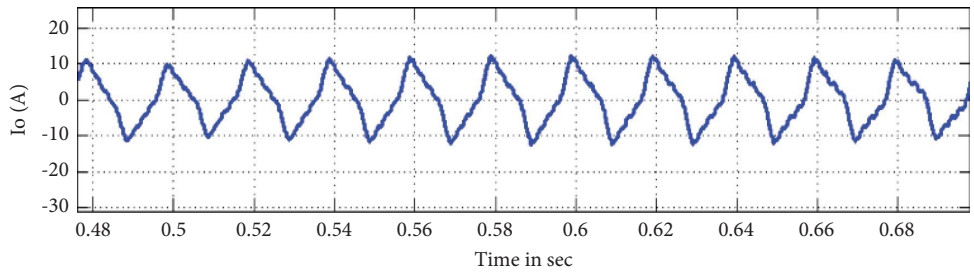

Figure 9: Output current through the closed-loop KBC-MLI converter scheme with source disturbance.

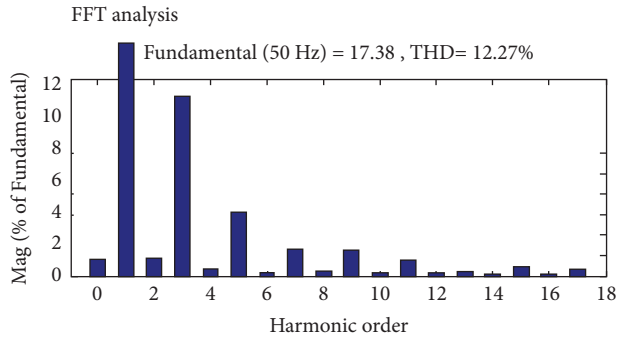

Figure 10: Output current THD with source disturbance.

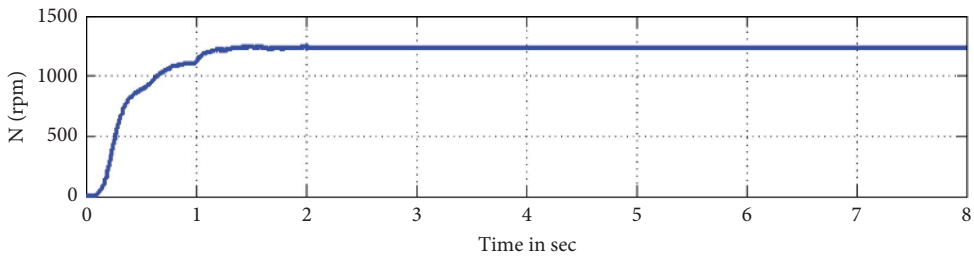

Figure 11: The motor speed of the closed-loop KBC-MLI converter structure with source disturbance.

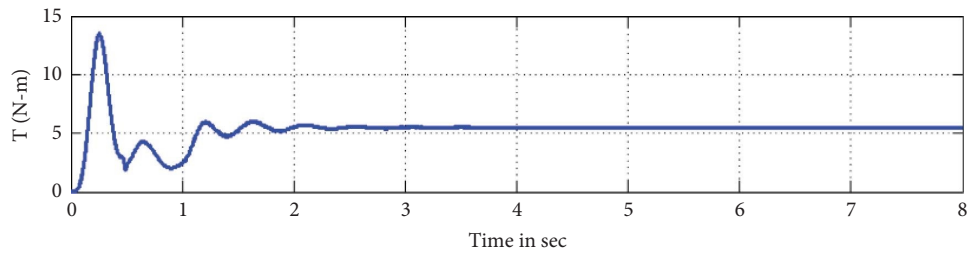

Figure 12: Motor torque of the closed-loop KBC-MLI converter system with source disturbance.

level inverter structures, the imbalanced operating time, as well as distribution of power, was recently addressed by employing phase-shifted PWM pulse-switching techniques.

5. Experimental Results

The single-phase KBC-MLI-based PV inverter system hardware snapshot is displayed in Figure 32. The voltage through PV has been illustrated in Figure 33. The switching pulse of KBC M_1 and M_2 is shown in Figure 34. These switching pulses are used to drive the controller circuit. The voltage across KBC has been displayed in Figure 35. The switching pulse of MLI S_1 and S_3 is shown in Figure 36. The output voltage across MLI and output current through the motor load are displayed in Figures 37 and 38, respectively. Table 3 summarizes the list of components used for simulation and hardware of the KBC-MLI system.

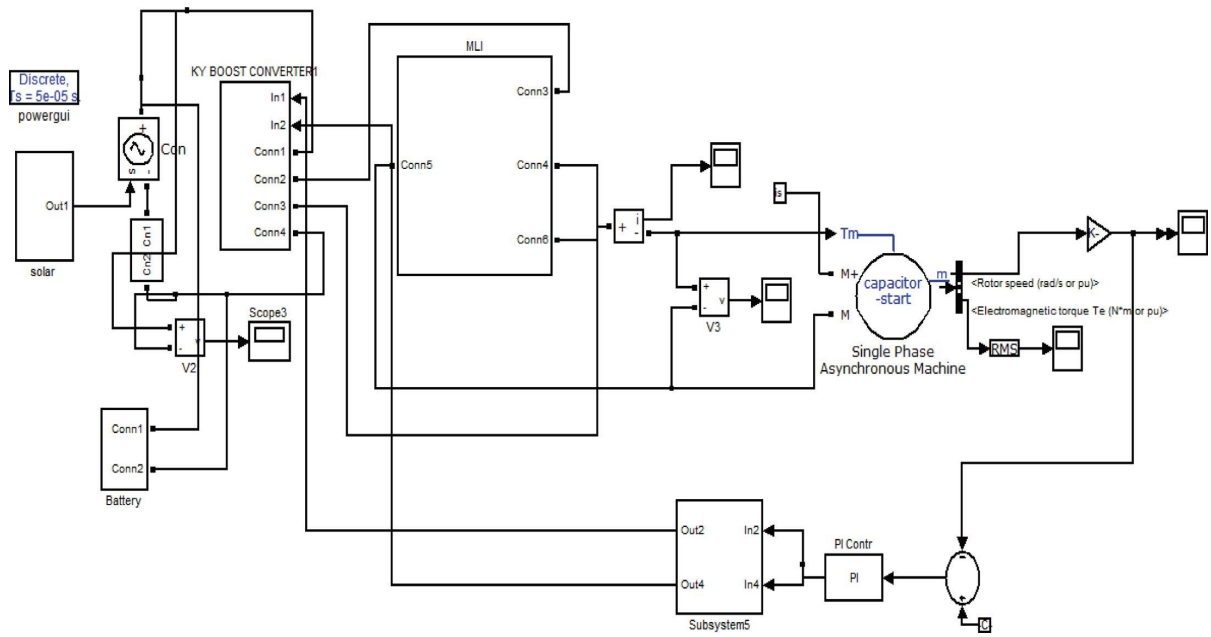

Figure 13: Circuit diagram of the closed-loop KBC-MLI system with a PI controller.

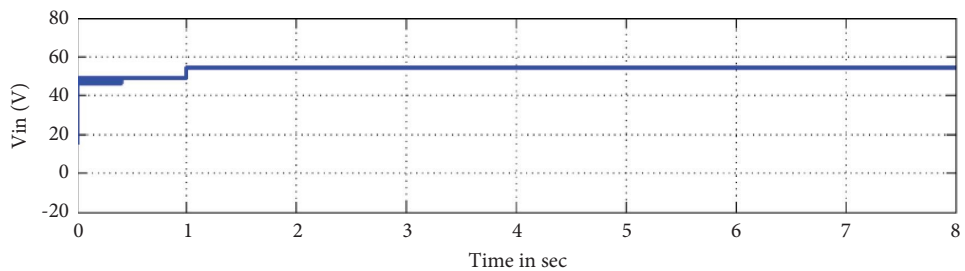

Figure 14: Solar PV voltage.

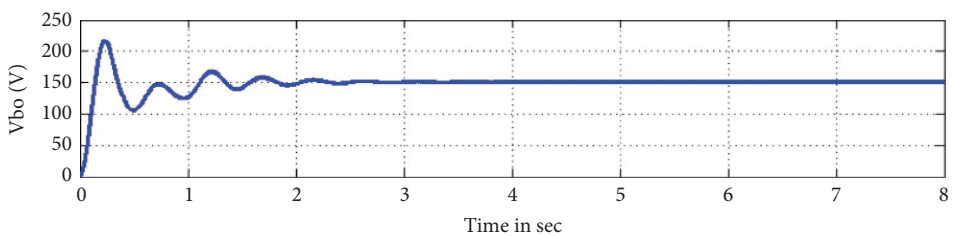

Figure 15: Output voltage of the closed-loop KBC-MLI structure with PI controller.

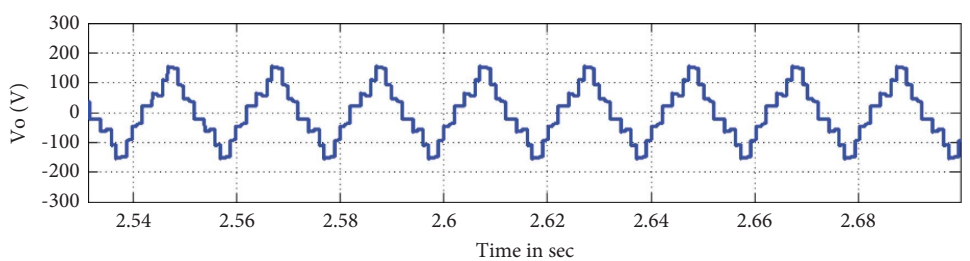

Figure 16: Output voltage across the motor of the closed-loop KBC-MLI structure with a PI controller.

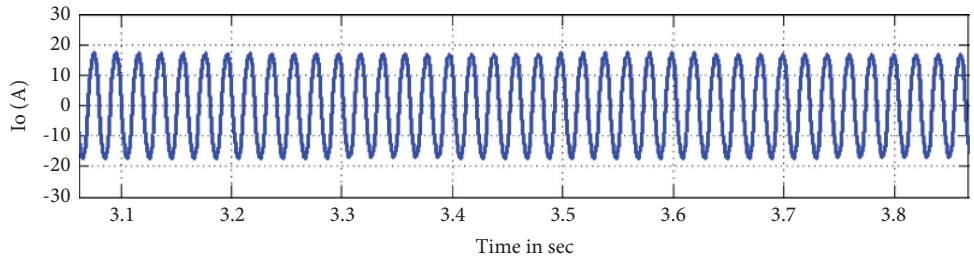

Figure 17: Output current through the closed-loop KBC-MLI converter system with a PI controller.

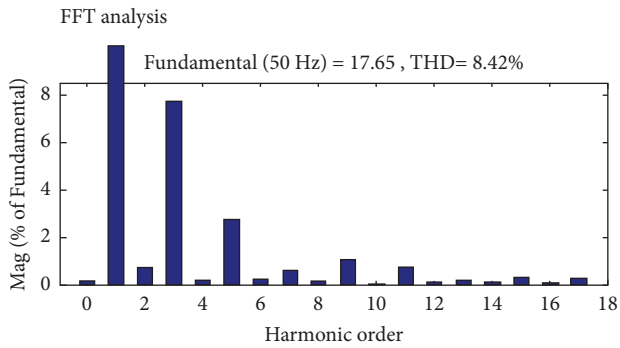

Figure 18: Output current THD with a PI controller.

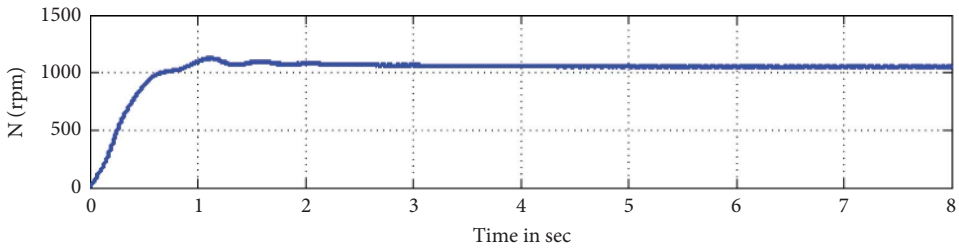

Figure 19: The motor speed of the closed-loop KBC-MLI converter structure with a PI controller.

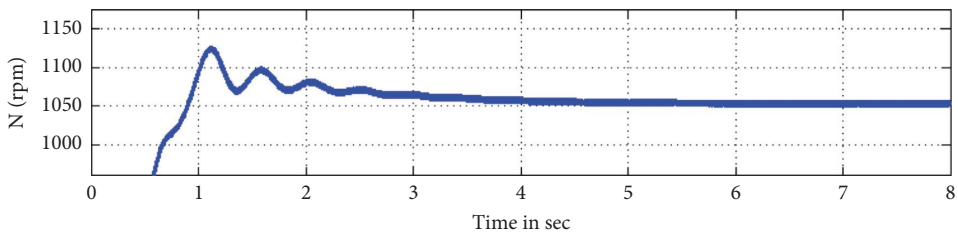

Figure 20: Motor speed zoom-out of the closed-loop KBC-MLI converter structure with a PI controller.

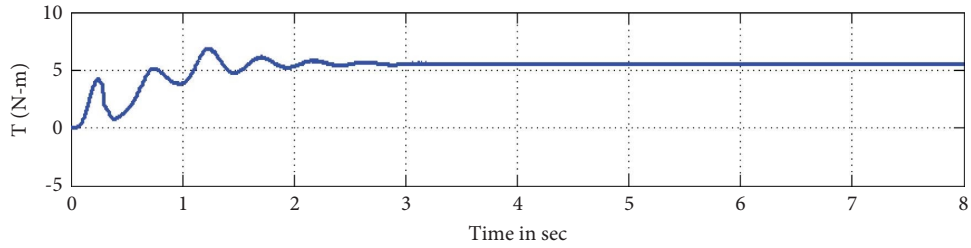

Figure 21: Motor torque of the closed-loop KBC-MLI converter system with a PI controller.

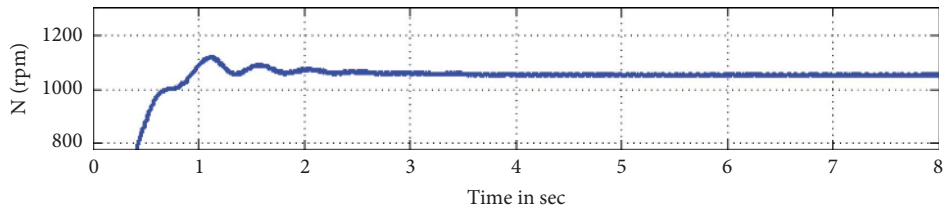

Figure 22: Motor speed zoom-out of the closed-loop KBC-MLI converter structure using the PI controller.

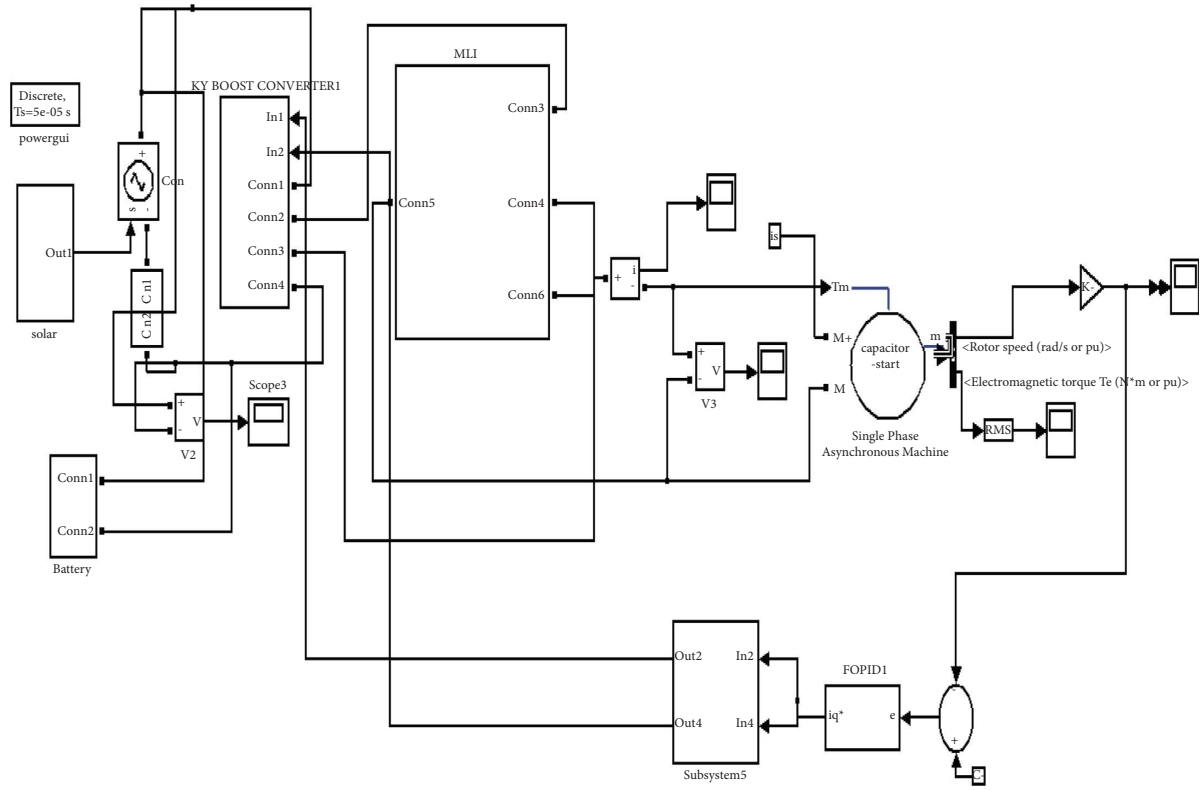

Figure 23: Schematic representation of the closed-loop KBC-MLI system using the FOPID controller.

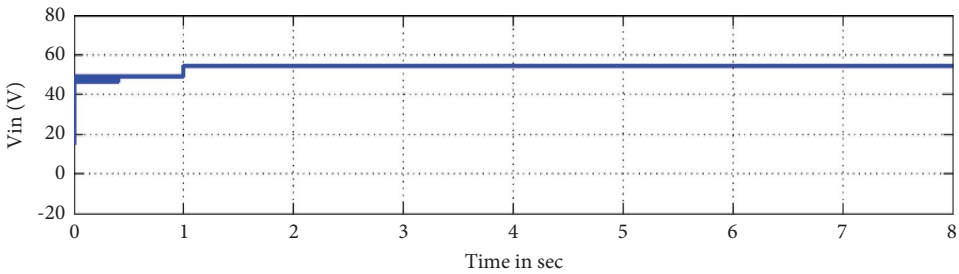

Figure 24: Voltage across PV.

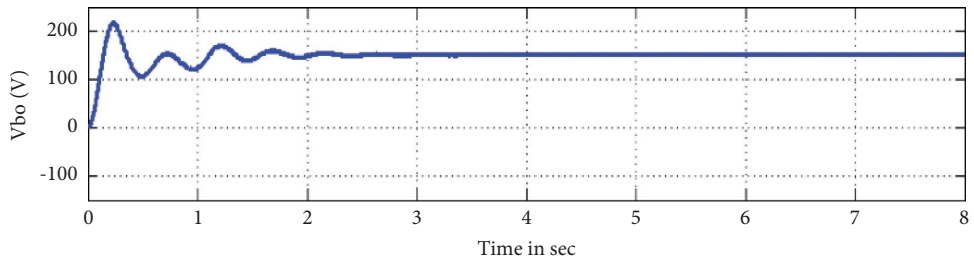

Figure 25: The output voltage across the motor of the closed-loop KBC-MLI structure using the FOPID controller.

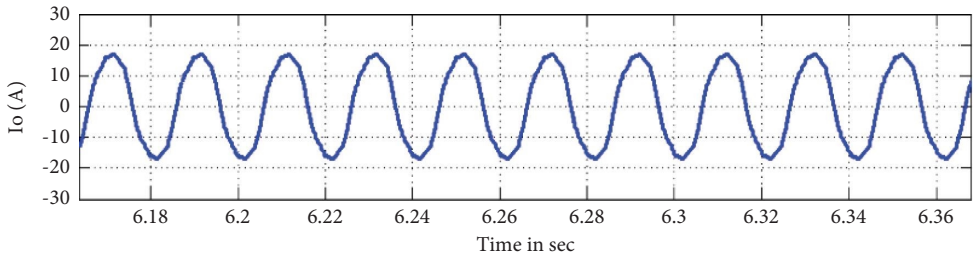

Figure 26: Output current through the closed-loop KBC-MLI converter structure using the FOPID controller.

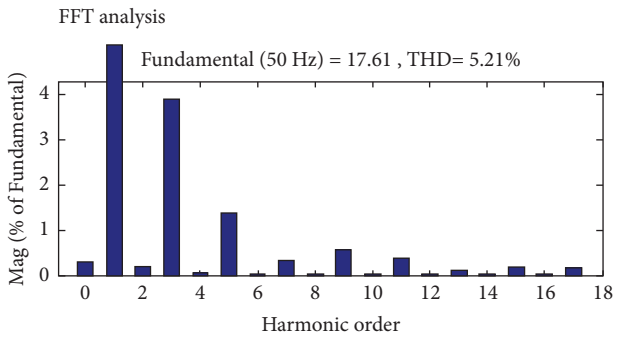

Figure 27: Output current THD with a FOPID controller.

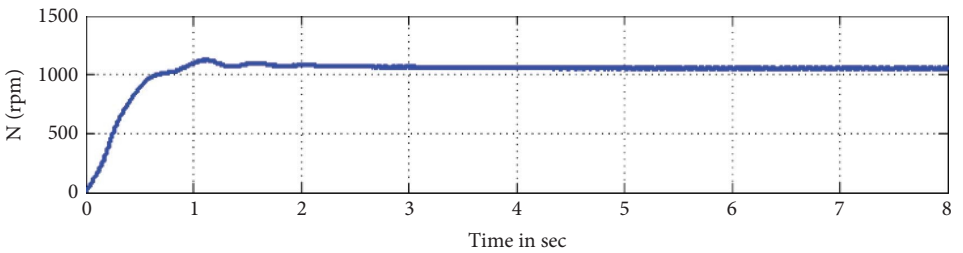

Figure 28: The motor speed of the closed-loop KBC-MLI converter structure using the FOPID controller.

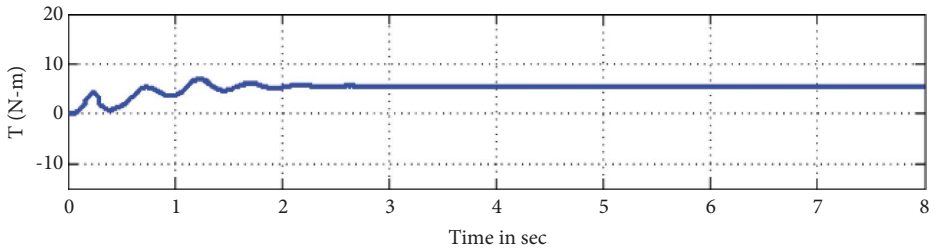

Figure 29: Motor torque of the closed-loop KBC-MLI converter structure using the FOPID controller.

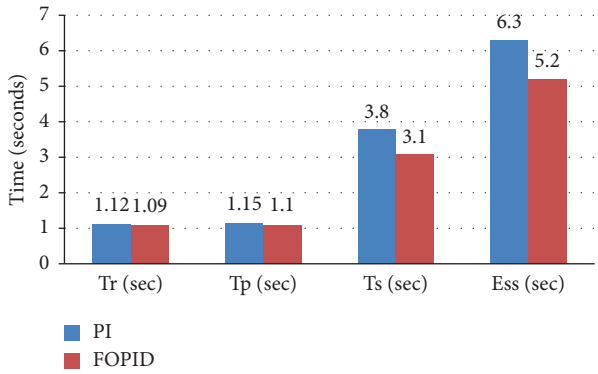

Figure 30: The bar chart of the PI and FOPID controllers with motor speed response.

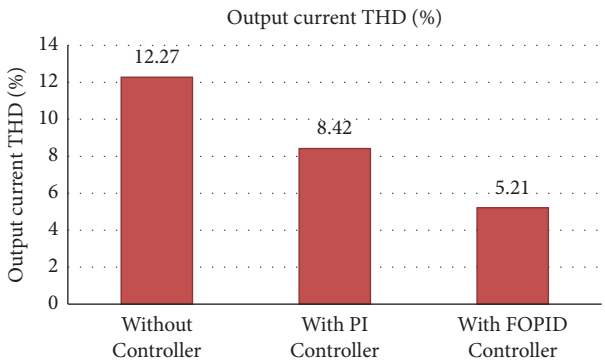

Figure 31: The bar chart of output current THD response.

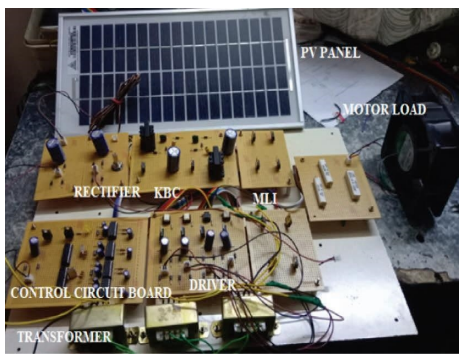

Figure 32: Hardware snapshot of the KBC-MLI converter.

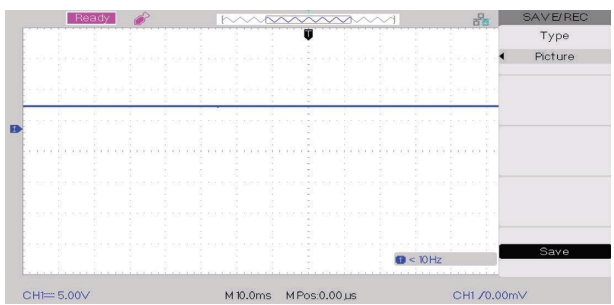

Figure 33: Input voltage.

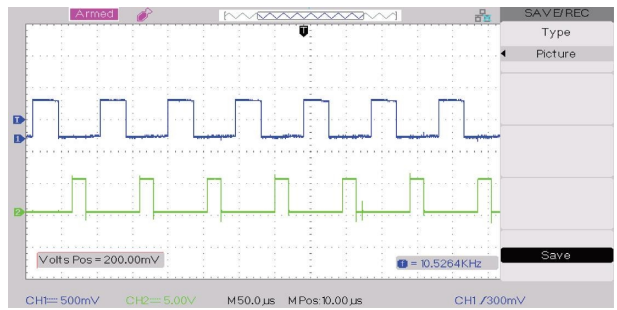

Figure 34: Switching pulses for M1 and M2 of the KY boost converter.

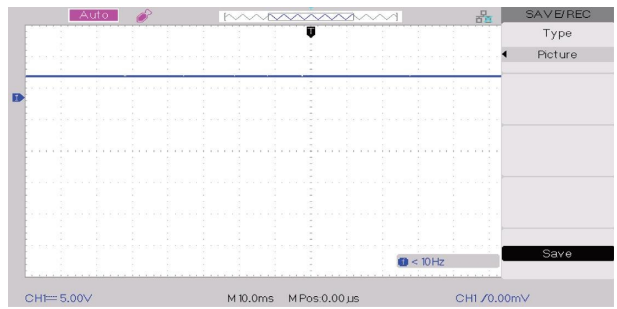

Figure 35: The voltage across the KY boost converter.

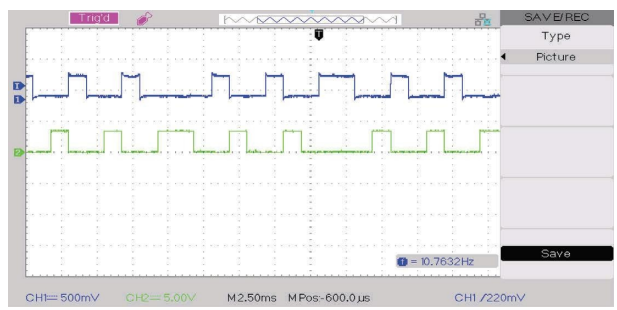

Figure 36: Switching pulse of multilevel inverters S1 and S3.

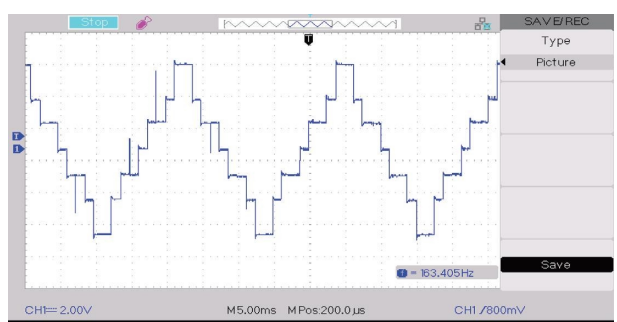

Figure 37: Voltage across motor load.

Figure 39 displays the output voltage spectra for every H-bridge preceding the net outputs on a comparable scale.

Power sharing in the cascaded 7-level inverter system in H-bridge-1 and H-bridge-2 output power is shown in Figure 40.

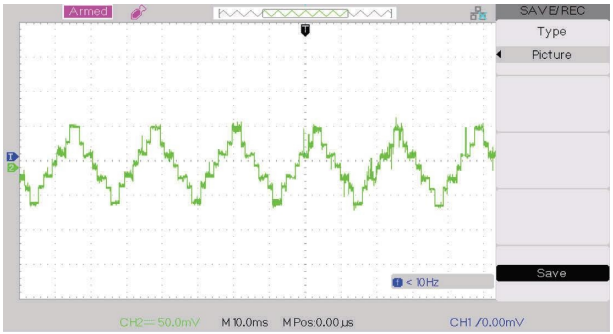

Figure 38: Current through motor load.

Table 3: List of components used for simulation and hardware of the KBC-MLI system.

Component	Simulation	Hardware
Vin	48 V	48 V
Switching pulse	5 V	10 V
Frequency	1 Khz	1 Khz
MOSFET	IRF840	IRF840
Diode	IN4007	IN4007
C_1,C_3	2000 μF	2200 μF
C_2	500 μF	500 μF
L_1	2 μH	3 μH
Vo	150 V	145 V

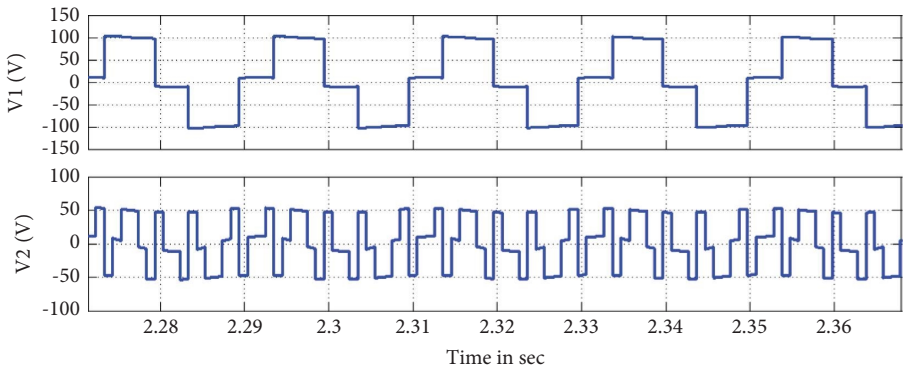

Figure 39: Output voltage waveforms of each H-bridge followed by net output in the same scale.

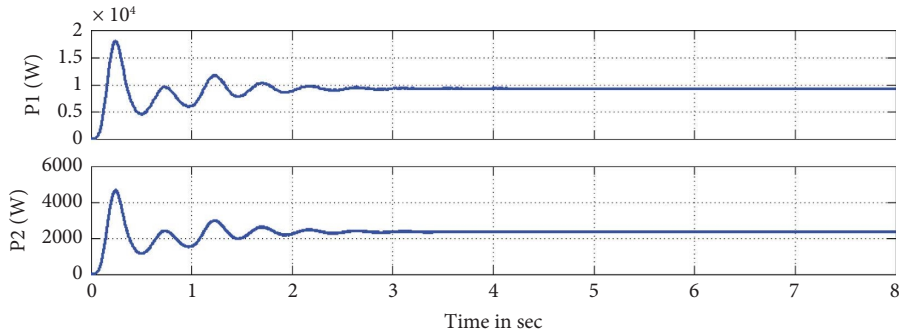

Figure 40: Power sharing in the cascaded 7-level inverter system in H-bridge-1 and H-bridge-2 output power.

6. Conclusions

For real-time machine tool applications using PI and FOPID controllers, simulation investigations involving open-loop source disturbance as well as closed-loop KBC-MLI systems were conducted. Simulink-based modeling for KBC-MLI structures has been utilized to conduct this investigation. The results showed that in comparison with the PI-controlled KBC-CMLI method utilized for machine tool uses, the closed-loop FOPID-controlled method delivered a decreased output current THD of 12.27% to 5.21% and enhanced time response for motor speed. Lower rising time and lowered settling time, as well as lower steady-state error voltage, are the advantages of the suggested KBC-CMLI method. The adoption of a closed-loop FOPID controller design has improved dynamic responsiveness. The hardware analysis coincides with the KBC-CML inverter systems' simulated outcomes. The main disadvantage of the KBC-CMLI method is the increase in device blocks incurred during the cascade. The analysis of PI and FOPID-controlled closed-loop KBC-MLI structures is the main focus of the current research. In the future, studies will analyze KBC-MLI structures with fuzzy logic controllers.

Abbreviations

BC:	Boost converter
BBC:	Buck-boost converter
CSC:	Canonical switching converter
FOPID:	Fractional order PID
FOC:	Field orientation control
IM:	Induction motors
IMD:	Induction motor drive
IMFOC:	Induction motor field orientation control
K_P, K_I, and K_D:	Controller
KBC:	KY boost converter
LC:	Inductor capacitor
MLI:	Multilevel inverter
PV:	Photovoltaic
PWM:	Pulse width modulation
SM:	Switched mode
SSI:	Solid-state inverter
THD:	Total harmonic distortion
V_o:	Output voltage
T_{on}:	On time
T_t:	Total time
λ:	Order of the integral part
μ:	Order of the derivative part.

Data Availability

The data used to support the findings of this study are available from the corresponding author upon request.

Conflicts of Interest

The authors declare that there are no conflicts of interest regarding the publication of this article.

Acknowledgments

All the expenses of this work are fully carried out at the author's own expense.

References

[1] A. Ramesh Babu, T. A. Raghavendiran, V. Sivachidambaranathan, and J. Barnabas Paul Glady, "Novel cascaded H-bridge sub-multilevel inverter with reduced switches towards low total harmonic distortion for photovoltaic application," *International Journal of Ambient Energy*, vol. 39, no. 2, pp. 117–121, 2018.

[2] P. Shanmuga Sundaram and A. Ramesh Babu, "Application of DSTATCOM for loss minimization in radial distribution system," *Proceedings of the International Conference on Soft Computing Systems, Advances in Intelligent Systems and Computing*, vol. 397, pp. 189–198, 2015.

[3] X. Liu, J. P. Xu, Z. Chen, and N. Wang, "Single inductor dual output buck-boost power factor correction converter," *IEEE Transactions on Industrial Electronics*, vol. 62, no. 2, pp. 943–952, 2015.

[4] Y. Li, Z. Zhu, Y. Yang, and C. Zhang, "An input-powered high-efficiency interface circuit with zero standby power in energy harvesting systems," *Journal of Power Electronics*, vol. 15, no. 4, pp. 1131–1138, 2015.

[5] D. Lee, "Simple MOSFET gating delay scheme for SMPS start-up in the standby power reduction circuit," *IET Power Electronics*, vol. 11, no. 1, pp. 16–22, 12 1 2018.

[6] M. Saravanan and A. R. Babu, "High power density multi-mosfet-based series resonant inverter for induction heating applications," *International Journal of Power Electronics and Drive Systems*, vol. 7, no. 1, pp. 107–113, 2016.

[7] S. Sreekanth and S. Gomathy, "Speed control of a three phase Induction motor using PI Control and Fuzzy logic control Method," *International Journal of Emerging Technology and Advanced Engineering*, 2015.

[8] D. R. Kumar and V. Geetha, "Simulation of single phase switching capacitor 49 level inverter with reduced THD," *International Journal of Engineering and Advanced Technology*, vol. 8, no. 6, pp. 837–841, 2019.

[9] S. Singh, B. Singh, G. Bhuvaneswari, V. Bist, A. Chandra, and K. Al-Haddad, "Improved-power-quality bridgeless-converter-basedmultiple-output SMPS," *IEEE Transactions on Industry Applications*, vol. 51, no. 1, pp. 721–732, 2015.

[10] H.-S. Kim, J. K. Kim, K. B. Park, H. W. Seong, G. W. Moon, and M. J. Youn, "On/Off control of boost PFC converters to improve light-load efficiency in paralleled power supply units for servers," *IEEE Transactions on Industrial Electronics*, vol. 61, no. 3, pp. 1235–1242, 2014.

[11] A. Ramesh Babu and T. A. Raghavendiran, "High voltage gain multiphase interleaved DC-DC converter for DC micro grid application using ıntelligent control," *Computers and Electrical Engineering*, vol. 74, pp. 451–465, 2019.

[12] S. Senthilkumar, MoazzamHaidari, G. Devi, and A. SagaiFrancisBritto, "Wireless bidirectional power transfer for E-vehicle charging system," in *Proceedings of the International Conference on Edge Computing and Applications (ICECAA)*, pp. 13–15, IEEE, Tamilnadu, India, October 2022.

[13] M. L. Dhola, C. C. Shah, and S. L. Kaila, "Power factor improvement using Boost converter," *International Journal of Advance Engineering and Research Development (IJAERD)*, vol. 1, no. 3, pp. 1–4, 2014.

[14] K. Anitha, R. Chatterjee, T. Ramadevi, P. A. Rao, and K. Ravikanth, "Analysis of active power factor correction using single and dual mode boost converter," *International Journal of Electronics Engineering Research*, vol. 3, no. 2, pp. 38–44, 2015.

[15] V. Mohan, N. Stalin, and S. Jeevananthan, "A tactical chaos based PWM technique for distortion restraint and power spectrum shaping in induction motor drives," *International Journal of Power Electronics and Drive Systems*, vol. 5, no. 3, pp. 383–392, 2015.

[16] M. S. Mollik, M. A. Hannan, M. S. Reza et al., "The advancement of solid-state transformer technology and its operation and control with power grids: a review," *Electronics*, vol. 11, no. 17, p. 2648, 2022.

[17] G. Krithiga and V. Mohan, "Elimination of harmonics in multilevel inverter using multi-group marine predator algorithm-based enhanced RNN," *International Transactions on Electrical Energy Systems*, vol. 2022, Article ID 8004425, pp. 1–13, 2022.

[18] G. Chitrakala, N. Stalin, and V. Mohan, "Normally bypassed cascaded sources multilevel inverter with RGA optimization for reduced output distortion and formulaic passive filter design," *Journal of Circuits, Systems, and Computers*, vol. 29, no. 02, pp. 1–21, Article ID 2050019, 2019.

[19] G. Chitrakala, N. Stalin, and V. Mohan, "A segmented ladder structured multilevel inverter for switch count remission and dual-mode savvy," *Journal of Circuits, Systems, and Computers*, vol. 27, no. 14, Article ID 1850223, 2018.

[20] S. Sivamani and V. Mohan, "A three-phase reduced switch count multilevel inverter topology," *International Transactions on Electrical Energy Systems*, vol. 2022, Article ID 6193731, pp. 1–16, 2022.